

Supporting information to the manuscript

Relaxation time prediction for a light switchable peptide by molecular dynamics

Robert Denschlag^{*}, Wolfgang J. Schreier[†], Benjamin Rieff^{*},
Tobias E. Schrader[†], Florian O. Koller[†], Luis Moroder[‡], Wolfgang Zinth[†],
and Paul Tavan^{*§}

^{*}Theoretische Biophysik, Department für Physik,

[†]Lehrstuhl für Biomolekulare Optik and Munich Center for Integrated Protein Science CIPSM,

^{*†}Ludwig-Maximilians-Universität, Oettingenstr. 67, 80538 München, Germany

[‡]Max Planck Institut für Biochemie, Am Klopferspitz 18a, 82152 Martinsried, Germany

[§]corresponding author, email: tavan@physik.uni-muenchen.de,
phone: +49-89-2180-9220, fax: +49-89-2180-9202

Convergence of REST free energy maps

To study the convergence of the REST simulations listed in table 1 we have divided for each simulation the set of 10 replicas into two subsets each containing five replicas. 300 K data were collected for each of these subsets, whenever one of its replicas happened to visit the 300 K temperature rung. Thus, the two replica swarms $\kappa = 1, 2$ generated two independent 300 K data sets for which the conformational landscapes $G_\kappa(H_1, H_2)$ were calculated as described in Methods.

Already a first visual comparison of the various graphs labeled with the subscripts 1 and 2 in Figure 12 demonstrates a close similarity between the free energy landscapes $G_\kappa(H_1, H_2)$ extracted from the two different swarms $\kappa = 1, 2$ at 300 K. For the C22 force field (Figs. 12a $_{\kappa}$, b $_{\kappa}$) the match between the landscapes $G_\kappa(H_1, H_2)$ associated to the swarms κ is very good apart from small differences between the depths of the various local minima. For CMAP (Figs. 12c $_{\kappa}$, d $_{\kappa}$) the match of the data from the two subsets is not quite as impressive but still pretty good. The modifications of the landscapes induced by the application of different force fields, which are discussed in the paper in connection with Fig. 3, are clearly retained in the swarm landscapes. For instance, both C22 swarms predict for the *cis* ensemble nearly no occupancy in the region $H_1 > 0.6$ (cf. Figs. 12a $_1$, a $_2$) and substantial occupation of the region $H_1 > -0.6$, whereas the CMAP swarms show the opposite behavior (cf. Figs. 12c $_1$, c $_2$). Thus, the differences of the conformational landscapes attributed in the paper to differences between the force fields are definitely not artifacts of insufficient statistics. Furthermore, the sampling of the conformational spaces as expressed by the complete data sets seems to be pretty exhaustive.

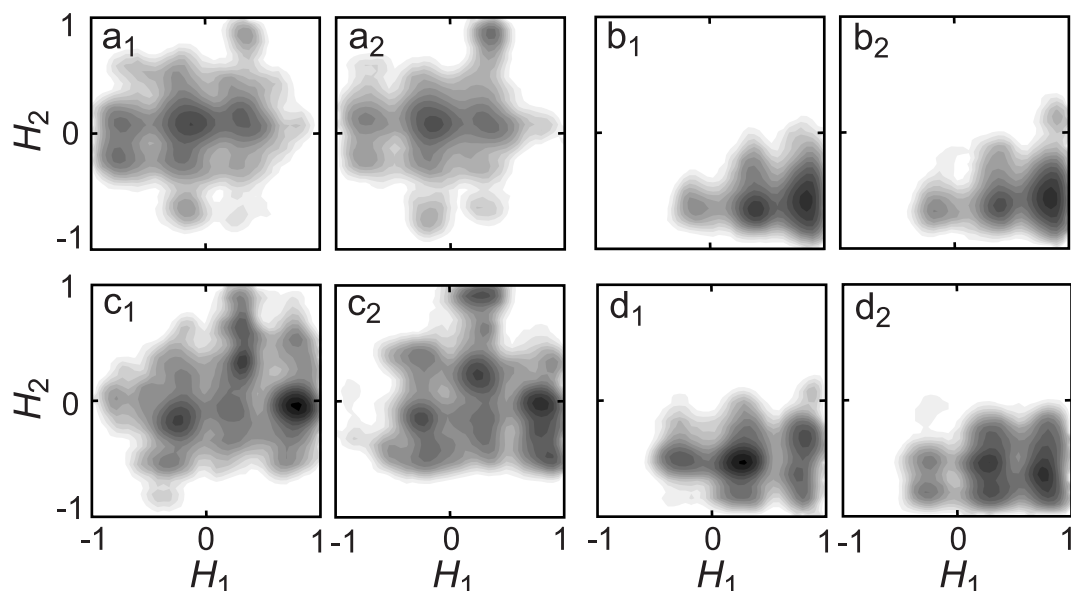


Figure S12: Free energy landscapes $G_\kappa(H_1, H_2)$ obtained at 300 K from two different swarms $\kappa = 1, 2$ covering five replicas each. Swarm 1 contains the replicas with initial temperatures in the range [300 K, 399 K], and swarm 2 those from [428 K, 570 K]. Results of swarm κ are depicted in the graphs labeled with the subscript κ . With the nomenclature of table 1 the graphs refer to the following simulations: (a $_{\kappa}$) R/C/C22, (b $_{\kappa}$) R/T/C22, (c $_{\kappa}$) R/C/CMAP, and (d $_{\kappa}$) R/T/CMAP.

Differences of the force fields. The C22 and CMAP force fields yield different predictions for 300 K equilibrium ensembles of cAPB in the *cis*- and *trans*-states. Because Fig. S12 has demonstrated that all our REST simulations (cf. table 1) yield well-converged the free energy landscapes $G_\kappa(H_1, H_2)$, the differences between the two predictions can be identified by a visual comparison between the top (C22) and bottom (CMAP) rows of Fig. 3 (or equivalently of Fig. S12). All differences, which are discussed in detail below and are detectable in Fig. 3, are statistically significant, indeed.

For the *trans* ensemble (Figs. 3b,d or Figs. 12b $_{\kappa}$, d $_{\kappa}$) both force fields apparently agree that the central part of the peptide backbone is largely extended ($H_2 < 0$). Correspondingly, the averages $\bar{H}_{2,t}$ have very similar values (cf.

table 2). Slight conformational differences are predicted by C22 and CMAP, respectively, for the peptide backbone near the covalent linkages to the chromophore. Within the dominant conformational substate resulting from C22, this portion of the backbone is seen to exhibit sharper turns ($H_1 \approx 0.8$) than in the corresponding CMAP state ($H_1 \approx 0.3$). Similarly the ensemble average \bar{H}_1 is by about 0.3 larger for C22 than for CMAP.

With respect to the conformational coordinate H_1 the *cis* ensembles show the opposite behavior: CMAP predicts that highly populated conformational substates are located in the region $H_1 > 0.6$, which corresponds to substantial turns at the linkages (cf. Fig. 3c). Thus also the average $\bar{H}_1 = 0.38$ is positive and close to the value of 0.40 found for the CMAP *trans* ensemble. In contrast, C22 predicts that the "turn" region $H_1 > 0.6$ of the conformational space is essentially empty (cf. Fig. 3a). Instead the region $H_1 < -0.6$ signifying extended structures at the linkages is well-populated. As a result, for C22 the average value \bar{H}_1 is shifted to the smaller value of -0.09 . In contrast, CMAP assigns only a very small population to the "extended" region $H_1 < -0.6$. Concerning the helicity of the core of the peptide (as measured by H_2) the Figs. 3a,c reveal no significant differences for the two force fields. This visual impression is validated by the values of $\bar{H}_{2,c}$ which are very similar indeed (cf. table 2).

As a result, the two force fields predict slightly different conformational ensembles for *cis*- and *trans*-CAPB at 300 K with the differences being largely confined to the linkage regions within which the peptide is covalently attached to chromophore.

Proton distances

In the following two tables S4 and S5 the proton distances from experiment,¹ earlier MD simulations² and our REST simulations are listed. Table S4 contains the *cis* data and table S5 the *trans* data.

Force Field:		—	C22		CMAP		
Temperature:		300 K	500 K	300 K	570 K	300 K	570 K
Atom 1	- Atom 2 ^a	r_{exp}^b	r_{MD}^c	r_{MD}^d	r_{MD}^d	r_{MD}^e	r_{MD}^e
APB:0:H2,H4	- ALA:1:HN	4.52	2.69	2.73	2.72	2.73	2.72
APB:0:H1,H5	- ALA:1:HN	6.71	4.72	4.77	4.75	4.78	4.75
ALA:1:HA	- CYS:2:HN	3.01	2.79	2.54	2.55	2.75	2.58
ALA:1:HB*	- CYS:2:HN	4.07	2.86	2.93	2.93	3.44	3.37
ALA:1:HB*	- ALA:3:HN	5.08	4.82	4.56	4.45	4.87	4.46
CYS:2:HA	- ALA:3:HN	2.88	2.58	2.56	2.70	2.70	2.54
CYS:2:HN	- ALA:1:HN	3.11	2.67	3.18	2.81	2.63	2.44
ALA:3:HA	- THR:4:HN	2.81	2.63	2.63	2.60	2.40	2.50
ALA:3:HB*	- THR:4:HN	4.32	3.03	2.99	3.02	3.66	3.47
ALA:3:HB*	- APB:0:H1,H5	7.86	6.15	10.55	7.87	5.86	6.42
ALA:3:HB*	- APB:0:H6,H10	8.03	6.16	11.06	8.08	5.53	6.81
ALA:3:HB*	- APB:0:H7,H9	7.21	5.34	9.52	6.56	4.30	5.73
ALA:3:HN	- CYS:2:HN	3.09	2.67	2.61	2.34	2.31	2.33
THR:4:HA	- CYS:5:HN	2.77	2.62	2.58	2.48	2.57	2.47
THR:4:HB	- CYS:5:HN	3.30	2.78	2.65	2.61	3.18	3.02
THR:4:HG2*	- APB:0:H1,H5	8.02	6.80	7.64	7.52	7.78	7.72
THR:4:HG2*	- APB:0:H6,H10	7.33	6.67	6.87	7.83	7.42	7.70
THR:4:HG2*	- APB:0:H7,H9	6.79	5.90	5.63	7.34	6.23	6.74
THR:4:HN	- ALA:3:HN	3.28	2.84	2.72	2.58	2.74	2.44
THR:4:HN	- CYS:5:HN	3.20	2.70	2.76	2.65	2.28	2.45
ASP:6:HA	- GLY:7:HN	2.94	2.56	2.61	2.53	2.73	2.52
ASP:6:HB1	- THR:4:HG1	4.80	6.22	6.94	6.47	6.38	5.66
ASP:6:HB2	- THR:4:HG1	4.80	5.24	5.61	5.18	5.91	4.86
ASP:6:HB1	- GLY:7:HN	5.30	2.74	2.68	2.57	3.33	3.05
ASP:6:HB1	- PHE:8:HPHE*	7.10	5.47	5.58	6.06	5.96	5.81
ASP:6:HB2	- PHE:8:HPHE*	7.10	5.81	6.10	6.57	6.28	6.26
ASP:6:HB1	- APB:0:H7,H9	6.20	6.05	6.46	5.90	6.70	5.96
ASP:6:HB2	- APB:0:H7,H9	6.78	6.43	7.04	6.10	7.56	6.88
GLY:7:HA1	- ASP:6:HA	4.90	4.51	4.54	4.52	4.76	4.57
GLY:7:HA2	- ASP:6:HA	5.02	4.57	4.59	4.54	4.62	4.53
GLY:7:HA1	- PHE:8:HN	3.24	2.47	2.47	2.41	2.88	2.59
GLY:7:HA2	- PHE:8:HN	3.24	2.72	2.55	2.69	2.97	2.67
GLY:7:HN	- ASP:6:HN	3.00	2.67	2.56	2.51	2.64	2.35
PHE:8:HA	- APB:0:H7,H9	6.01	4.24	4.23	4.29	4.48	4.35
PHE:8:HA	- APB:0:HN	2.53	2.49	2.47	2.54	2.85	2.65
PHE:8:HB1	- APB:0:H7,H9	6.92	4.68	4.80	4.70	4.77	4.71
PHE:8:HB2	- APB:0:H7,H9	6.78	4.38	4.20	4.29	4.23	4.23
PHE:8:HB1	- APB:0:HN	3.47	2.78	2.94	2.77	2.78	2.75
PHE:8:HB2	- APB:0:HN	3.80	2.60	2.45	2.52	2.50	2.46
PHE:8:HN	- APB:0:HN	3.35	2.68	2.78	2.49	2.45	2.47
PHE:8:HPHE*	- APB:0:HN	6.54	4.79	5.21	5.07	5.49	5.14
RMSV ^f :		-	0.23	0.81	0.29	0.34	0.14

Table S4: Proton distances r for *cis*-cAPB. ^aNames of the involved Atoms using the following nomenclature: Residue:Number:Atom(s) - Residue:Number:Atom(s). A star indicates a set of (chemically) equivalent protons. ^bexperiment. ^cCarstens et al. ^dREST simulation R/T/C22. ^eREST simulation R/T/CMAP. ^fRMSV. All distances are given in Å.

Force Field:		—	C22		CMAP		
Temperature:		300 K	500 K	300 K	570 K	300 K	570 K
Atom 1	- Atom 2 ^a	r_{exp}^b	r_{MD}^c	r_{MD}^d	r_{MD}^d	r_{MD}^e	r_{MD}^e
APB:0:H2,H4	- ALA:1:HN	4.70	2.65	2.72	2.71	2.71	2.71
ALA:1:HB*	- CYS:2:HN	4.02	2.90	2.91	2.95	3.44	3.30
ALA:1:HB*	- ALA:3:HN	5.80	5.25	5.21	5.15	5.68	5.37
CYS:2:HA	- ALA:3:HN	2.64	3.11	2.99	3.14	2.60	2.70
CYS:2:HB1	- ALA:3:HN	3.19	2.58	2.53	2.49	3.07	3.08
CYS:2:HB2	- ALA:3:HN	3.42	2.74	2.60	2.65	3.16	3.17
CYS:2:HN	- ALA:1:HN	2.63	2.29	2.38	2.25	2.27	2.14
ALA:3:HB*	- CYS:2:HA	5.22	5.37	5.45	5.47	5.18	5.22
ALA:3:HB*	- CYS:2:HN	5.42	5.50	5.41	5.20	5.10	4.82
ALA:3:HB*	- THR:4:HN	3.96	2.99	2.97	2.94	3.40	3.28
ALA:3:HB*	- APB:0:H1,H5	7.02	7.31	7.93	6.32	5.07	4.81
THR:4:HA	- CYS:5:HN	2.56	2.51	2.54	2.43	2.32	2.36
THR:4:HA	- APB:0:H1,H5	6.04	4.03	3.71	3.84	4.33	4.44
THR:4:HB	- CYS:5:HN	3.09	2.88	3.18	2.73	3.73	3.15
THR:4:HB	- ASP:6:HN	4.35	6.35	7.06	5.17	4.53	4.25
THR:4:HG2*	- ASP:6:HN	5.09	5.55	6.21	5.23	3.82	4.21
THR:4:HG2*	- APB:0:H6,H10	6.42	5.14	5.04	5.10	4.96	5.37
CYS:5:HB1	- ASP:6:HN	3.28	2.64	2.37	2.47	3.39	2.93
CYS:5:HB2	- ASP:6:HN	3.63	2.92	3.01	2.72	3.41	3.22
CYS:5:HB1	- APB:0:H6,H10	6.29	4.10	4.98	4.31	5.07	4.64
CYS:5:HB2	- APB:0:H6,H10	6.06	4.39	3.70	3.95	4.71	4.41
CYS:5:HB2	- APB:0:H7,H9	6.83	5.01	4.27	4.36	5.21	4.79
ASP:6:HA	- GLY:7:HN	2.82	2.36	2.39	2.45	2.29	2.41
ASP:6:HB1	- THR:4:HG1	4.79	6.55	7.59	6.66	4.36	5.29
ASP:6:HB2	- THR:4:HG1	4.63	5.95	7.47	5.74	4.18	4.52
ASP:6:HB1	- GLY:7:HN	3.60	2.54	2.36	2.40	2.76	2.65
ASP:6:HB2	- GLY:7:HN	3.64	2.87	3.27	2.70	3.67	3.11
ASP:6:HB1	- APB:0:H6,H10	7.20	6.63	7.18	5.92	4.79	5.56
ASP:6:HB2	- APB:0:H6,H10	7.20	6.59	7.25	5.58	4.71	5.13
ASP:6:HB1	- APB:0:H7,H9	6.80	5.47	5.89	5.19	3.68	4.60
ASP:6:HB2	- APB:0:H7,H9	6.80	5.75	6.40	4.98	4.23	4.54
ASP:6:HB1	- APB:0:HN	5.62	4.98	5.53	4.64	3.22	3.96
GLY:7:HN	- ASP:6:HN	3.86	3.40	3.96	2.92	3.27	2.53
GLY:7:HA1	- ASP:6:HA	4.67	4.46	4.56	4.50	4.42	4.45
GLY:7:HA2	- ASP:6:HA	4.40	4.49	4.46	4.52	4.41	4.51
GLY:7:HA1	- PHE:8:HN	2.71	2.25	2.19	2.27	2.52	2.35
GLY:7:HA2	- PHE:8:HN	3.13	3.18	3.22	3.12	3.18	2.99
GLY:7:HA1	- APB:0:HN	4.28	3.91	3.82	3.93	4.34	4.05
GLY:7:HA2	- APB:0:HN	4.58	4.96	5.08	5.03	4.90	4.95
PHE:8:HB1	- APB:0:HN	3.64	2.75	2.59	2.70	2.50	2.76
PHE:8:HB2	- APB:0:HN	3.79	2.78	2.72	2.62	2.69	2.63
PHE:8:HN	- APB:0:HN	2.86	2.36	2.29	2.30	2.43	2.39
PHE:8:HPHE*	- APB:0:HN	6.50	5.31	5.77	5.49	5.68	5.44
RMSV ^f :		-	0.47	0.72	0.45	0.13	0.10

Table S5: Proton distances r for *trans*-cAPB. ^aNames of the involved Atoms using the following nomenclature: Residue:Number:Atom(s) - Residue:Number:Atom(s). A star indicates a set of (chemically) equivalent protons. ^bexperiment. ¹ ^cCarstens et al. ² ^dREST simulation R/T/C22. ^eREST simulation R/T/CMAP. ^fRMSV. All distances are given in Å.

Force field parameters of the chromophore

The following four tables S6, S7, S8, and S9 contain the force field parameters for the APB switch and for its covalent linkage to the peptide. Fig. S13 shows the chemical structure of the APB chromophore. The mapping between the atom names given in the figure and the atom types required for specifying the force field is given in table S6.

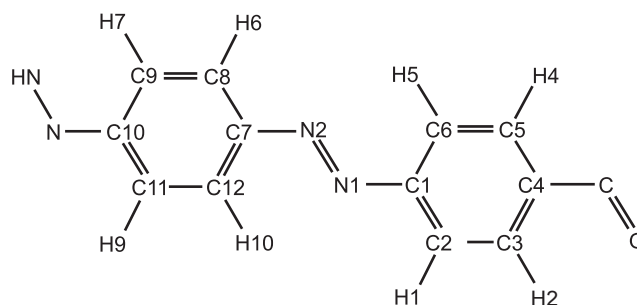


Figure S13: Chemical structure of the APB chromophore. The mapping between atom names and atom types is given in table S6.

Name	Atom type	Charge	Name	Atom type	Charge
C1	CAZ	0.4028	C2	CAZ	-0.2561
C3	CAZ	-0.0145	C4	CAZ	-0.1647
C5	CAZ	-0.0145	C6	CAZ	-0.2561
N1	NAZ	-0.2439	N2	NAZ	-0.2439
C7	CAZ	0.4028	C8	CAZ	-0.1803
C9	CAZ	-0.2389	C10	CAZ	0.3665
C11	CAZ	-0.2389	C12	CAZ	-0.1803
H1	HAZ	0.1202	H2	HAZ	0.0836
H4	HAZ	0.0836	H5	HAZ	0.1202
H6	HAZ	0.1202	H7	HAZ	0.1654
H9	HAZ	0.1654	H10	HAZ	0.1202
N	NH1	-0.5293	HN	H	0.3192
C	C	0.5930	O	O	-0.5017

Table S6: Partial charges derived by DFT.³

Type 1	Type 2	k_b	b_0
CAZ	CAZ	419.4	1.398
NAZ	CAZ	341.7	1.419
HAZ	CAZ	404.7	1.086
NAZ	NAZ	716.8	1.261
C	CAZ	250.0	1.504
NH1	CAZ	320.0	1.405
CT2	CAZ	230.0	1.526

Table S7: Atom types, force constant k_b (kcal mol⁻¹ Å⁻²), and equilibrium distance b_0 (Å) defining the covalent bond energy terms.³

Type 1	Type 2	Type 3	k_ϕ	ϕ_0
CAZ	CAZ	CAZ	40.0	120.0
HAZ	CAZ	CAZ	34.4	120.0
NAZ	CAZ	CAZ	60.2	120.0
NAZ	NAZ	CAZ	121.1	114.8
C	CAZ	CAZ	45.8	120.0
O	C	CAZ	80.0	121.0
NH1	C	CAZ	80.0	116.5
NH1	CAZ	CAZ	70.0	120.0
H	NH1	CAZ	35.0	114.8
C	NH1	CAZ	50.0	120.0
HA	CT2	CAZ	49.3	107.5
CT2	CAZ	CAZ	45.8	120.0
NH1	CT2	CAZ	50.0	116.3

Table S8: Atom types, force constant k_ϕ (kcal mol⁻¹ rad⁻²), and equilibrium angle ϕ_0 (deg) defining the angles energy terms.³

Type	Type	Type	Type	k_{ϕ_n}	n	ϕ_n
CAZ	NAZ	NAZ	CAZ	12.47	2	180.0
NAZ	NAZ	CAZ	CAZ	2.03	2	180.0
				0.18	4	0.0
CAZ	CAZ	C	X	0.55	2	180.0
				0.13	4	0.0
C	CAZ	CAZ	CAZ	3.10	2	180.0
CAZ	C	NH1	CT1	1.60	1	0.0
				2.50	2	180.0
CAZ	C	NH1	H	2.50	2	180.0
CAZ	CAZ	NH1	X	0.71	2	180.0
				0.13	4	0.0
NH1	CAZ	CAZ	CAZ	3.10	2	180.0
CT1	C	NH1	CAZ	1.60	1	0.0
				2.50	2	180.0
O	C	NH1	CAZ	2.50	2	180.0
CAZ	NAZ	NAZ	CAZ	20.62	2	180.0
				3.19	4	0.0

Table S9: Atom types, force constant k_{ϕ_n} (kcal/mol), periodicity n , and phase shift (deg) for dihedral energy terms defining the dihedral energy terms. The parameters for the dihedral CAZ-NAZ-NAZ-CAZ given at the bottom of the table are used in the MD/ISOM3 simulation.³

Temperature dependence and other properties of the RMSV

Based on a very simple model we explain, why the observable RMSV, which is defined by Eq. (8) and is used to measure the agreement between NMR proton-proton distances d_{ij}^{exp} and simulation data, is expected to be a monotonously decreasing function of the simulation temperature T (as is apparent in Fig. 6).

Assume that a peptide is in the solid state, i.e., that the peptide atoms i thermally fluctuate around fixed average positions $\langle \mathbf{r}_i \rangle$. If the fixing is harmonic, then the standard deviation of the fluctuations increases with \sqrt{T} (in the limit of small amplitudes) and the positions $\mathbf{r}_i(t)$ are normally distributed. Therefore, also the distances $r_{ij}(t)$ between the atoms will be normally distributed

$$p(r_{ij}|\sigma_{ij}) = \frac{1}{\sqrt{2\pi}\sigma} \exp\left[-\frac{(r_{ij} - \langle r_{ij} \rangle)^2}{2\sigma_{ij}^2}\right] \quad (1)$$

around average distances $\langle r_{ij} \rangle$ with standard deviations σ_{ij} increasing monotonously with \sqrt{T} . Then the so-called interaction distances d_{ij} , which are defined by Eq. (7) and serve for comparisons of simulation data with NOE distance restraints d_{ij}^{exp} , can be estimated through

$$d_{ij} \equiv \left[\left\langle \frac{1}{r_{ij}^6} \right\rangle \right]^{-1/6} \approx \left[\int_{r_{\min}}^{\infty} \frac{p(r_{ij}|\sigma_{ij})}{r_{ij}^6} dr_{ij} \right]^{-1/6} \quad (2)$$

where the minimal distance r_{\min} models a hard-sphere exclusion applicable to close atoms. Because the widths σ_{ij} of the distance distributions $p(r_{ij})$ are functions of T , also the interaction distances d_{ij} depend on T .

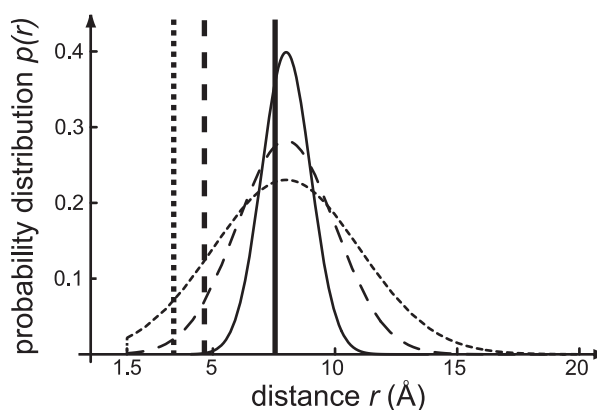


Figure S14: Distance distributions $p(r_{ij}|\sigma_{ij})$ of two hydrogen atoms in a putative rigid model structure for three different temperatures T_{κ} . Low temperature T_1 : solid; intermediate temperature T_2 : dashed; high temperature T_3 : dotted. Also indicated through the vertical bars are the associated NMR interaction distances $d_{ij,\kappa}$.

As a specific example, consider two hydrogen atoms for which a NOE signal has been measurable. Then the experimental distance d_{ij}^{exp} of these atoms will be not much larger than about 5 Å, because NOE signals of more distant atoms become very weak. Now suppose that the average distance $\langle r_{ij} \rangle$ in the simulated (rigid) structure is 8 Å and that the contact distance r_{\min} is 1.5 Å. Consider furthermore three different temperatures T_{κ} , $\kappa = 1, 2, 3$, as measured by the three different widths $\sigma_{ij,\kappa} = 1, 2, 3$ Å, and assume that the average distances $\langle r_{ij} \rangle$ are independent of temperature as is approximately the case for solids with a small thermal expansion coefficient. Then the corresponding interaction distances $d_{ij,\kappa}$ resulting from the three different distance distributions shown in Fig. S14 are 7.51, 4.66, and 3.29 Å, respectively. Thus, the interaction distances $d_{ij,\kappa}$ monotonously decrease with increasing temperatures T_{κ} although the average structure is invariant ($\langle r_{ij} \rangle = 8$ Å).

Next suppose that the measured distance d_{ij}^{exp} is 4 Å. Then the contributions $\max[0, d_{ij,\kappa} - d_{ij}^{\text{exp}}]^2$ of the three interaction distances $d_{ij,\kappa}$ to the RMSV are 12.3 Å², 0.4 Å², and 0, respectively (cf. the definition of the RMSV in

Eq. (8)). Thus, although the average structures in the three simulations are identical, the low temperature simulation correctly signifies a large deviation for this particular distance whereas the high temperature simulation signifies no violation at all. High temperature simulations like those in Ref. 2 can therefore give the incorrect impression of a good match with NMR data. This artifact is avoided by choosing the experimental temperature in the simulations.

In summary, the simple model of a harmonically fixed and, thus, **rigid peptide structure** clearly explains why one should expect a monotonously decreasing RMSV, if one simulates the system at increasing temperatures. Note in this context that the experimental distances d_{ij}^{exp} should have the same temperature dependence as the interaction distances d_{ij} derived from a simulation implying that one will measure smaller values with increasing T (as long as the structure remains rigid). If one wants to use the RMSV as an absolute measure for judging the quality of a model structure, one has to make sure that the thermal fluctuations in the experimental and simulated systems are of equal size.

The above example has also shown that the interaction distances d_{ij} decrease, if more small values r_{ij} are contained in the ensemble of sampled distances. For a **multimodal** distance distribution $p(r_{ij})$ featuring many substates, which is the generic case for **flexible peptides**, this property implies that the interaction distance d_{ij} is dominated by the substates exhibiting small distances. If one finds, e.g., nine times the value $r_{ij} = 8 \text{ \AA}$ and once the value $r_{ij} = 2 \text{ \AA}$, then Eq. (7) predicts an interaction distance $d_{ij} \approx 3 \text{ \AA}$.

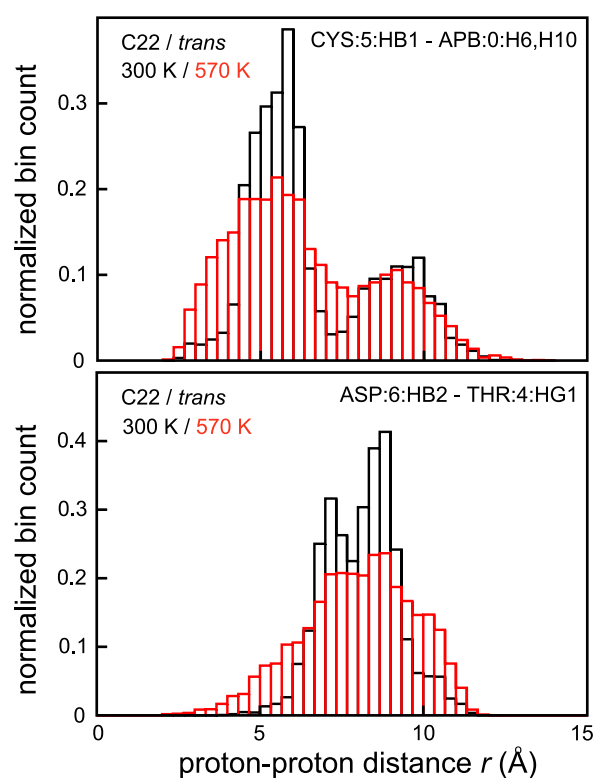


Figure S15: Histograms of distance distributions $p(r_{ij}|\sigma_{ij})$ for hydrogen atoms observed in REST simulations of *trans*-cAPB at two different temperatures.

Finally we want to demonstrate that the simple model actually applies to cAPB. In Figure 15 we provide examples for the temperature dependencies of two randomly selected proton-proton distance distributions, for which NOE's were actually observed in *trans*-cAPB (see table S5 for the corresponding interaction distances d_{ij}). The two histograms both show broadenings of the respective distributions upon heating and nearly invariant locations, around which they are centered. In particular, both distributions feature an increasing number of small distances upon heating which explains, why the associated interaction distances decrease from 4.98 to 4.31 Å for the top histogram and from 7.47 to 5.74 Å for the bottom histogram with increasing T . Because in the former case the

observed distance is 6.29 Å and, thus, larger than the MD interaction distances at both temperatures, the contributions to the RMSV vanish in both cases (cf. Eq. 8). In the latter case, however, it is small measuring only 4.63 Å and, hence, the contribution to the RMSV decreases with T . Because relatively small distances are frequent among the NMR data, the monotonous decrease of the total RMSV with increasing T is readily understood.

Note here that the bimodal distribution (top) reflects the existence of at least two conformations in the simulated ensemble. As mentioned above, the NOE interaction distance is 6.29 and, thus, right at the location of the first maximum of the 300 K distance distribution shown in the top graph of Fig. S15 indicating again that NOE distances overlook substates with large proton-proton distances.

Temperature dependence of average helicity scores

Whereas the shapes of the amide I bands in the spectra of peptides are highly sensitive to the temperature, the ensemble average helicity \bar{H}_2 of *cis*-cAPB is nearly independent of temperature. This fact is proven by Fig. S16 for the CMAP force field, which shows the variation of \bar{H}_2 within the generalized REST ensemble as a function of the temperature.

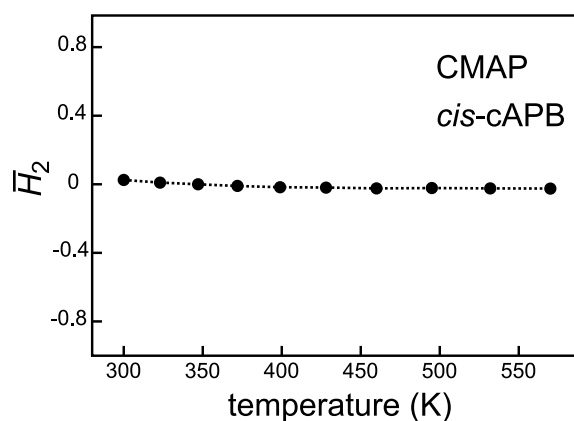


Figure S16: The ensemble average helicity \bar{H}_2 of *cis*-cAPB as a function of temperature within the REST simulation R/C/CMAP.

Fast cooling processes monitored by MD

Because the observable $\bar{H}_2(t)$ is insensitive to the temperature and senses the structural alteration of the chromophore, which is caused by its *cis/trans* isomerization, only with a delay of about 100 ps, the faster relaxation processes are overlooked by $\bar{H}_2(t)$. In contrast, the peptide's temperature directly maps the initial deposition of heat into the peptide and its subsequent dissipation into the surrounding solvent. For an ensemble of 500 short (100 ps) simulations of the cAPB photoisomerization in DMSO, where the peptide was described by the C22 force field, we have monitored the ensemble average time course of cAPB's temperature $\bar{T}(t)$.

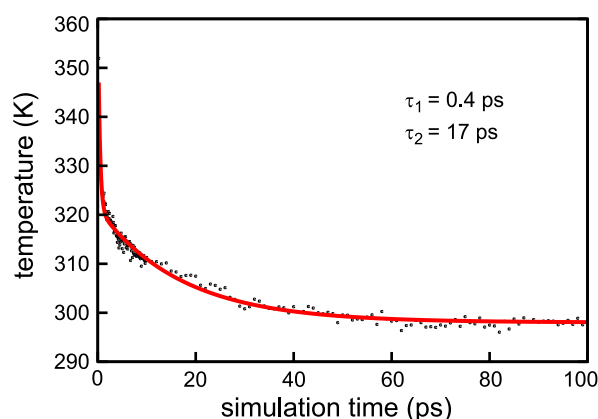


Figure S17: Temporal evolution $\bar{T}(t)$ of cAPB's average temperature extracted from an ensemble of 500 short simulations of the *cis/trans* photoisomerization.

Fig. S17 shows these data together with a fit using a sum of two exponential functions. This fit yields a fast decay of 0.4 ps corresponding to the immediate ballistic dissipation of energy during the chromophore's isomerization and a slower cooling process occurring on a time scale of 17 ps. The former time constant roughly agrees with the 0.3 ps kinetics extracted from cAPB's total energy calculated in earlier MD simulations and with the 0.2 ps time constant determined by ultrafast pump-probe spectroscopy in the UV/vis region for the chromophore isomerization.⁵ The latter time constant nicely agrees with the 11 ps kinetics observed in the time resolved amide I spectra of cAPB (see table 3) and with earlier measurements of such cooling kinetics by optical pump-probe spectroscopy,⁶ which determined a cooling time of 15 ps for hot azobenzene in ethanol.

Slow relaxation processes monitored by MD

Fig. S11 in the paper shows the time resolved landscapes $G[H_1, H_2, t]$ at the time points $t/\text{ns} \in \{0, 0.2, 2, 20\}$. For a simple numerical representation of these distributions we additionally provide in table 10 the average linkage and core helicities $\bar{H}_1(t)$ and $\bar{H}_2(t)$, respectively. The table demonstrates once again that only $\bar{H}_2(t)$ is suited to distinguish *cis* and *trans*.

time/ns	C22 ^a		CMAP ^b	
	\bar{H}_1	\bar{H}_2	\bar{H}_1	\bar{H}_2
$-\infty$	-0.09	0.10	0.38	0.03
0.2	0.13	-0.02	0.28	-0.12
2.0	0.30	-0.26	0.43	-0.22
20	0.47	-0.44	0.31	-0.40
∞	0.67	-0.56	0.40	-0.54

Table S10: Temporal evolution of average helicities $\bar{H}_i(t)$, $i = 1, 2$. ^aFrom simulation I/C22 for $|t| < \infty$, R/C/C22 for $t = -\infty$, and R/T/C22 for $t = \infty$. ^bFrom I/CMAP for $|t| < \infty$, R/C/CMAP for $t = -\infty$, and R/T/CMAP for $t = \infty$.

Relaxation plotted on a logarithmic time scale

The simulated kinetics of the *cis/trans* relaxation of cAPB as monitored by the average helicity score $\bar{H}_2(t)$ in the core of the peptide has been presented on a linear time axis in Fig. S10. This linear plot clearly reveals the slow ($\tau_3 = 23$ ns) exponential decay but does not resolve the fast processes associated with τ_1 and τ_2 . Therefore we plot in Fig. S18 the same data once again on a logarithmic time scale.

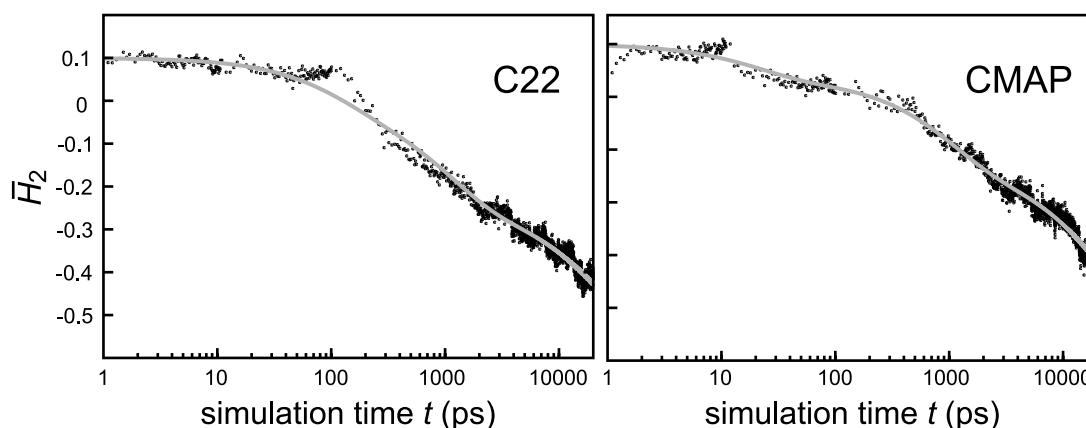


Figure S18: Data on the simulated *cis/trans* relaxation of cAPB from Fig. S10 presented on a logarithmic time scale to clearly resolve the fast events.

For the C22 force field, the average core helicity $\bar{H}_2(t)$ is essentially invariant during the first 150 ps, although the isomerization is finished after 0.3 ps, and cooling as well as important conformational changes occur within this time in the vicinity of the chromophore.⁵ This observation demonstrates that it takes a certain amount of time until the stretching of the chromophore propagates to the core of the peptide. After about 150 ps the average helicity score $\bar{H}_2(t)$ of the peptide core suddenly drops indicating the force-driven unfolding of the one α -helix in the *cis*-ensemble.

For CMAP the results are qualitatively similar, but the first unfolding of one of the two α -helices in the *cis*-ensemble occurs already after 10 ps. A second sharp drop after about 150 ps indicates the sudden breaking of the hydrogen bonds stabilizing the second α -helix in the ensemble. The fact that the fast processes mainly involve individual unfolding events explains, why the very fast time constants τ_1 determined by the multi-exponential fits bear large statistical uncertainties.

References

- [1] C. Renner, R. Behrendt, S. Spörlein, J. Wachtveitl and L. Moroder, *Biopolymers*, 2000, **54**, 489–500.
- [2] H. Carstens, C. Renner, A. G. Milbradt, L. Moroder and P. Tavan, *Biochemistry*, 2005, **44**, 4829–4840.
- [3] H. Carstens, *Dissertation*, Fakultät für Physik, Ludwig-Maximilians-Universität München, 2004.
- [4] X. Daura, K. Gademann, H. Schafer, B. Jaun, D. Seebach and W. F. van Gunsteren, *J. Am. Chem. Soc.*, 2001, **123**, 2393–2404.
- [5] S. Spörlein, H. Carstens, H. Satzger, C. Renner, R. Behrendt, L. Moroder, P. Tavan, W. Zinth and J. Wachtveitl, *Proc. Natl. Acad. Sci. USA*, 2002, **99**, 7998–8002.
- [6] T. Naegle, R. Hoche, W. Zinth and J. Wachtveitl, *Chem. Phys. Lett.*, 1997, **272**, 489–495.